Eur. Phys. J. Spec. Top.
https://doi.org/10.1140/epjs/s11734-024-01101-w

THE EUROPEAN PHYSICAL JOURNAL SPECIAL TOPICS

Review

Cosmic neutrino background: a minireview

Ujjal Kumar Dey[a]

Department of Physical Sciences, Indian Institute of Science Education and Research Berhampur, Transit Campus, Govt. ITI, Engg. School Junction, Berhampur, Odisha 760010, India

Received 15 September 2023 / Accepted 19 January 2024

Abstract The standard model of cosmology, i.e., the big bang theory, along with cosmic microwave background (CMB), also predicts the existence of a cosmic neutrino background (CνB). This CνB is comprised of ultra low energy neutrinos. Their detection can provide us the information about the Universe at a stage earlier than the CMB can provide. In this short review, we present basic theoretical properties and constraints on CνB and subsequently present a quick review of the experimental proposals for its detection. In addition to this, we also discuss the effect of generalized neutrino interactions on the CνB detection via the neutrino capture process at PTOLEMY.

1 Introduction

Along with boosting a dynamic program in the particle physics sector, neutrinos play an equally crucial role in the frontiers of cosmology. The standard model of cosmology, i.e., the ΛCDM, predicts in in addition to cosmic microwave background (CMB) the presence of a cosmic neutrino background (CνB) [1]. In the standard picture of ΛCDM, the neutrinos got decoupled from the thermal bath (~ 1 s after the Big Bang) earlier than the CMB photons ($\sim 4 \times 10^5$ years) and formed CνB. Detection of these neutrinos can thus show us the Universe at the earliest possible epoch after the Big Bang. The contribution of the CνB neutrinos in the energy density of the Universe affects the light element abundances during big bang nucleosynthesis (BBN) and leaves its signatures in the CMB anisotropies, and structure formation. These early Universe observations constitutes indirect signatures of CνB and put some bounds on it. More precisely, cosmological observations like BBN, baryon acoustic oscillation, CMB as well as observations from neutrino experiments constrain some of the features of CνB. However, due to the tiny masses, small interaction cross sections, and current low-temperature of the CνB ($T_{\nu,0} \sim 1.95$ K) it is extremely difficult to detect the CνB neutrinos directly. Even then many novel proposals to detect CνB neutrinos have been put forward. Based on the proposal by Weinberg [2], the Princeton Tritium Observatory for Light, Early-Universe, Massive-Neutrino Yield (PTOLEMY) experiment has been set up to detect CνB neutrinos by capturing electron neutrinos on a 100 g tritium target via the process $^3\mathrm{H} + \nu_e \rightarrow {}^3\mathrm{He}^+ + e^-$ [3]. Some other interesting proposals include, Stodolsky effect [4, 5], usage of different types of interferometer [6, 7], bremsstrahlung processes [8], annual modulation due to gravitational focusing by the sun [9], coherent neutrino scattering [10–13], resonant scattering with cosmogenic neutrinos [14], atomic de-excitation [15], accelerator experiments [16], spectral lines from possible neutrino decays [17] etc.

In the next section, we briefly elaborate on the theoretical understanding of the origin of CνB by following the thermal history of neutrinos. In Sect. 3 we mention some of the constraints on CνB coming from astrophysical/cosmological and experimental observations. In Sect. 4 we describe a few detection possibilities, laying more emphasis on the neutrino capture process since this is the basic process to be used by PTOLEMY. Finally we summarise and discuss a few future directions.

[a] e-mail: ujjal@iiserbpr.ac.in (correspondingauthor)

2 A brief (thermal) history of ν

At the primordial hot and dense stage of the Universe, neutrinos maintained an equilibrium with the SM thermal bath which was constituted mostly of electrons, positrons, and photons, via the weak interactions. Clearly, this hindered their free-streaming. These interactions were various scattering and annihilation processes, e.g., $e^- e^+ \rightleftharpoons \nu_j \bar{\nu}_j$, $e^{\pm}\nu_j \rightleftharpoons e^{\pm}\nu_j$, $e^{\pm}\bar{\nu}_j \rightleftharpoons e^{\pm}\bar{\nu}_j$. A quick order-of-magnitude estimation of such cross sections σ can easily be obtained by noting the interaction strength, weak mediators, etc. as, $\sigma \sim \alpha^2 E_\nu^2 / m_{W,Z}^4$, where α is the fine structure constant, $m_{W,Z}$ is the mass of the weak gauge bosons and E_ν is the neutrino energy. The relevant interaction rate can be calculated from the thermal average of the cross section, $\langle\sigma v\rangle$ and the number density of the neutrinos, i.e., $\Gamma_{\rm int} = n\langle\sigma v\rangle$. Since at the concerned temperatures, neutrinos behave like ultra-relativistic particle species, the number density of neutrinos per degree of freedom is, $n = 3\zeta(3)T^3/(4\pi^2)$. Noting that neutrinos travel at a velocity close to that of light, $v \sim c$ the typical neutrino energy is $E_\nu \sim T$. Thus the interaction rate becomes,

$$\Gamma_{\rm int} = n\langle\sigma v\rangle \sim \frac{\alpha^2}{m_{W,Z}^4} T^5 \sim G_F^2 T^5. \tag{1}$$

where $G_F \approx 1.2 \times 10^{-5}\text{GeV}^{-2}$ is the Fermi constant.

As the Universe expands and cools down, the neutrinos decouple from the thermal bath. The expansion rate of the Universe, which is parametrized by the Hubble parameter $H = \dot{a}/a$, where a is the scale factor, at the radiation-dominated epoch ($\rho \propto T^4$) is given by,

$$H = \frac{\dot{a}}{a} = \sqrt{\frac{8\pi G}{3}\rho} \sim \sqrt{\frac{8\pi G}{3} g_* \frac{\pi^2}{30} T^4} \sim \sqrt{g_*}\frac{T^2}{m_{Pl}} \propto T^2 \propto a^{-4}, \tag{2}$$

where G is the universal gravitational constant which in natural units defines the Planck mass scale, $m_{\rm Pl} = G^{-1/2} = 1.22 \times 10^{19}$ GeV, and g_* is the number of relativistic degrees of freedom which at that time gets contribution only from the photons, electrons, positrons, and neutrinos,

$$g_*(T) = \sum_{\rm B} g_b + \frac{7}{8}\sum_{\rm F} g_f = 2 + 4 \times \frac{7}{8} + 6 \times \frac{7}{8} = 10.75. \tag{3}$$

The neutrino decouples from the thermal plasma when $\Gamma_{\rm int} \lesssim H$. Thus from Eqs. (1) and (2), the freeze-out temperature for neutrinos $T_{\nu,f}$ can be evaluated,

$$\begin{aligned} &G_{\rm F}^2 T_{\nu,\rm f}^5 = \sqrt{g_*}\frac{T_{\nu,\rm f}^2}{m_{\rm Pl}} \Rightarrow T_{\nu,\rm f} = \left(\frac{\sqrt{g_*}}{G_{\rm F}^2 m_{\rm Pl}}\right)^{1/3} \sim g_*^{1/6}\,\text{MeV}, \\ &T_{\nu,\rm f} \sim 1.48\,\text{MeV}. \end{aligned} \tag{4}$$

Note that a more refined calculation predicts $T_{\nu_e,\rm f} \sim 2.3$ MeV, and $T_{\nu_\mu,\nu_\tau,\rm f} \sim 3.5$ MeV [18, 19], see also [20–22]. From this one can get the present effective neutrino temperature, $T_{\nu,0} = T_{\nu,\rm f} a(t_\nu)/a(t_0) = T_{\nu,\rm f}/(1+z_\nu)$, where z_ν is the redshift at the time of neutrino decoupling. At that time temperatures of the neutrinos and the photons were the same. But after the neutrino decoupling the thermal bath effectively was filled with electrons, positrons, and photons, of which the electrons and the positrons started to annihilate photons as soon as the temperature dropped below the electron mass, thereby injecting entropy into the photons. This increased the photon temperature higher than the effective neutrino temperature and consequently the photon decoupling occurred much later. This is the reason why the discovery of CνB can tell us about an epoch in which even CMB can not predict anything.

Now, using the fact that the entropy per co-moving volume is constant and $T_\nu \sim a^{-1}$, we can calculate the temperature of relic neutrinos as of today. Note that $s = g_* 2\pi^2 T^3/45$; $s_{e^\pm,\gamma} a^3 = \text{const.}$; $g_*(T)T^3/T_\nu^3 = \text{const.}$ For $T \gg m_e$, electrons and positrons are still relativistic, and $g_*^{e^\pm,\gamma}(T_{\nu,\rm f}) = 2 + 7 \times (2+2)/8 = 11/2$. After the e^+e^- annihilation, photons solely contribute to the entire entropy $g_*^\gamma(T_{\gamma,0}) \to 2$. During all this time neutrinos are present in the thermal soup. Just that after their decoupling they remained effectively non-interacting and following their own temperature, which falls as a^{-1}, tracks the photon temperature till the temperature dropped below $2m_e$ and most electrons and positrons annihilated. For temperatures well below electron mass, including the current epoch, we get

$$\frac{T_{\gamma,0}}{T_{\nu,0}} = \left(\frac{g_*^{e^\pm,\gamma}(T_{\nu,\rm f})}{g_*^\gamma(T_{\gamma,0})}\right)^{1/3} = \left(\frac{11}{4}\right)^{1/3} \simeq 1.4. \tag{5}$$

If we use the known value of the CMB temperature today, $T_{\gamma,0} = 2.725$ K [23], we see that neutrinos are as cold as $T_{\nu,0} = 1.945\,\mathrm{K}$, or 1.676×10^{-4} eV. Using the present temperature of neutrinos, we calculate the number density of neutrinos per degree of freedom to be $n_{\nu,0} = 3\zeta(3)T_{\nu,0}^3/4\pi^2 \simeq 56\,\mathrm{cm}^{-3}$. In conjunction with the oscillation experiments, the current temperature of neutrinos $T_{\nu,0} = 1.945\,\mathrm{K}$, necessitates that irrespective of normal or inverted hierarchy, at least two out of three mass eigenstates of neutrinos must be non-relativistic today. This brings in the issues of chirality, helicity, Dirac/Majorana etc., for a discussion see [24]. Thus detecting CνB can reveal certain neutrino properties which are otherwise difficult to measure at high momentum. Clearly, in all of these neutrinos are assumed to be stable.

In passing we also mention the clustering of neutrinos. Since neutrinos have some tiny masses they can not escape gravitational effects and, in principle, can be trapped by the gravitational potential wells of galaxies or their clusters if the CνB neutrinos have velocities smaller than the escape velocity [25]. This may lead to a local overdensity of neutrinos and the standard density of 56 cm^{-3} can be slightly enhanced [25, 26].

3 Constraints on CνB

After the basic introduction now we are going to discuss the constraints on CνB. These are obtained from various theoretical, experimental and observational considerations. The main point is that the neutrino density and temperature that we obtained earlier i.e., $(n_{\nu,0}, T_{\nu,0})$ assumes the standard (both from particle physics and cosmological point of view) evolution of the Universe. However, in the presence of additional degrees of freedom with possible late decays—democratically or exclusively to one eigenstate—to neutrinos will alter the obtained values of $(n_{\nu,0}, T_{\nu,0})$. This may lead to overdensities $(\eta_\nu = n_\nu/n_{\nu,0})$ in either per-eigenstate or the whole neutrino population. The above-mentioned considerations put bound on these overdensities. These constraints can be classified in two categories, namely the constraints coming from today's observations including neutrino oscillation experiments and cosmological constraints. In the following, we give a laconic summary of them, for a detailed discussion see [27].

3.1 Constraints from current epoch

Pauli exclusion principle: Due to their fermionic nature, local number density of neutrinos is subjected to the Pauli exclusion principle. Since the de Broglie wavelength of these relic neutrinos are macroscopic $\mathcal{O}(\mathrm{mm})$, by considering the momentum space available to these relic neutrinos one can constrain the overdensity η_ν.

Tremaine–Gunn bound: If the relic neutrinos are macroscopically clustered, they can be described by some coarse-grained distribution whose integration over momentum space gives the clustered neutrino density. The requirement that the maximum of this distribution does not exceed the usual Fermi-Dirac phase space density provides a bound on the overdensity. This is known as the Tremaine-Gunn bound. In some situations, this bound can be competitive as the Pauli exclusion bound.

Neutrino experiment: If due the presence of additional degrees of freedom and their decays, CνB neutrinos are sufficiently energetic they can be observed at existing neutrino experiments. Recent solar neutrino data from Borexino experiment [28] suggest that $T_{\nu_i} \lesssim 5$ keV. Data from neutrino mass measurement experiments utilising tritium beta decay such as KATRIN also put some constraints but the inference from the Borexino data is more robust.

3.2 Cosmological constraints

Relic neutrino overdensity at large redshifts can significantly alter the evolution of the Universe. If the relic neutrinos maintain their distribution from the time of decoupling, cosmological observations can put stringent bounds on the CνB overdensity today.

Big bang nucleosynthesis: The overdensity can be modeled by introducing a degeneracy parameter proportional to the chemical potential. This contributes to the effective number of neutrino species N_{eff}. In such a scenario big bang nucleosynthesis and subsequently structure formation can get affected. Therefore from the measurements of N_{eff} by various cosmological probes, e.g., Planck, one can put constraints on the neutrino temperature. Such bounds can in turn constrain the overdensity.

Baryon acoustic oscillation: After recombination, photons decoupled from the baryons and subsequently the pressure from the system is released. This created an overdensity of baryons at the scale of the acoustic horizon at recombination and the fluctuation of this overdensity constitutes what is known as baryon acoustic oscillation (BAO). Now, due to their high velocity neutrinos move significantly faster than sound waves in the hot plasma

and therefore propagate information ahead of the sound horizon of the plasma. This causes a phase shift in the BAO spectrum [29]. Therefore, from the astrophysical measurement of this spectrum constraints on CνB can be found.

CMB polarisation: In the early radiation dominated Universe, relic neutrino and photon scattered off each other. Since relativistic neutrinos are of mostly left helicity, the scattered CMB photons are polarised. This can contribute to the B-mode power spectrum of the CMB at large multipole moments [30]. Cosmological probes, e.g., Planck, BICEP, CMB-S4 etc. which can measure the B-mode spectrum can thus place bounds on the CνB.

4 Detection techniques

Detecting CνB neutrinos are challanging mainly for two reasons, first, since these neutrinos are usually non-relativistic their typical weak interaction cross section is extremely small; secondly the issue of threshold energy, i.e., traditional neutrino detection methods requires threshold (anti-)neutrino energies to be way higher than CνB neutrino energies, e.g., "inverse beta-decay" interactions with the protons in the water, producing positrons and neutrons requires anti-neutrinos with an energy above the threshold of 1.8 MeV.

However, one green shoot is that theoretical considerations show that CνB neutrino flux should be way too high [31]. In any case, any method of CνB detection requires, (i) removing or regulating the threshold, and (ii) enhance the event rate either by using exorbitantly large number of targets and/or increasing the cross sections. Keeping these essence, several methods to detect CνB have been proposed which broadly falls under three categories –

- indirect detection by finding spectral distortion through CνB interaction with ultra-high energy neutrinos or protons/nuclei from unknown sources;
- direct detection of coherent CνB elastic scattering with target nuclei through momentum transfer [mainly two types (a) $\mathcal{O}(G_{\rm F})$ effect (e.g., Stodolsky effect), (b) $\mathcal{O}(G_{\rm F}^2)$ effect (e.g., coherent neutral current scattering));
- direct detection by neutrino capture on β-decaying nuclei.

For illustration, in the following we will focus on some of the direct detection proposals and end the discussion with the most promising proposal of the neutrino capture by β-decaying nuclei.

4.1 Stodolsky effect ($\mathcal{O}(G_{\rm F})$)

This is one of the $\mathcal{O}(G_{\rm F})$ effect viable for the detection of CνB proposed by Stodolsky [4]. The idea is that the presence of a neutrino background can act as a potential that changes the energy of atomic electron spin states, somewhat analogous to the Zeeman effect in the presence of a magnetic field. The main requirements to have this energy splitting ΔE_e is that there should exist net neutrino chemical potential (for Dirac case) or net helicity (for Majorana case). In addition to this the relative motion of the Earth should not exceed the velocity of neutrinos in the CνB frame otherwise the helicity asymmetry can be washed out entirely. Moreover, the relative motion of the Earth cannot generate helicity asymmetry if there is none in the CνB frame. It can be shown that the energy splitting $\Delta E_e \sim G_{\rm F} g_A \beta_\oplus n_\nu$, where g_A is the axial-vector coupling the electron with the Z-boson and $\beta_\oplus$ is the relative velocity of the Earth with respect to the CνB frame.

The energy splitting ΔE_e can induce a torque $\tau_e \simeq \Delta E_e$ on each electron so that a ferromagnet with N_e number of polarised electrons in the presence of CνB experiences a total torque $N_e\tau_e \sim N_A Z M |\Delta E_e|/(A m_A)$, where N_A is Avogadro number, Z and A are the atomic and mass number of the target material, respectively, M is the total target mass and $m_A = 1$ g mol^{-1}. This can be utilised to induce a linear acceleration a on a ferromagnet with some spatial extent R as, $a \sim N_e \tau_e I$, where I is the concerned moment of inertia.

Given the current accuracy available in Cavendish-type torsion balance (with all possible improvements the smallest detectable acceleration $\sim 10^{-23}$ cm s^{-2}), even with the optimistic neutrino overdensity (producing $a_N \sim 10^{-26}$ cm s^{-2}) it is not yet feasible to use this idea to detect CνB neutrinos. However, with an increased sensitivity of torsion balance this method can not only be competitive with the neutrino capture method but also complement it since this method carries important information about the helicities of neutrinos.

4.2 Coherent Scattering ($\mathcal{O}(G_{\rm F}^2)$)

As the Earth moves through the sea of CνB neutrinos, a target on Earth experiences momentum transfer from neutrinos by elastic scattering. In the Earth's rest frame the momentum transfer per scattering is given by [5],

$$\langle \Delta p \rangle_{\rm R} \approx \beta_\oplus \frac{E_\nu}{c} \text{ for relativistic } \nu, \tag{6}$$

$$\langle \Delta p \rangle_{\rm NC,NR} \approx \beta_\oplus \frac{4T_\nu}{c} \text{ for non-clustering non-relativistic } \nu, \tag{7}$$

$$\langle \Delta p \rangle_{\rm C,NR} \approx \beta_\oplus c m_\nu \text{ for clustering non-relativistic } \nu. \tag{8}$$

Due to this momentum transfer there can be a small macroscopic acceleration a_N in a target with total mass M, $a_N = \Gamma_N \langle \Delta p \rangle / M$, where $\Gamma_N = N_T \beta_\nu \sigma_N n_\nu$ is the neutrino scattering rate, here σ_N is the coherent neutrino-nucleus scattering cross section. However, the coherence can be maintained over a single nucleus, i.e. for neutrino wavelengths $\lambda_{\nu_i} = 2\pi/|\vec{p}_{\nu_i}|$ of order the nuclear radius. For the ultra-nonrelativistic CνB neutrinos this condition is valid and thus it leads to an enhanced cross section. Usually,

$$\sigma_N \approx \begin{cases} 10^{-56} \left(\frac{m_\nu}{\rm eV}\right)^2 \,{\rm cm}^2 \text{ for non-relativistic } \nu, \\ 5 \times 10^{-63} \left(\frac{T_\nu}{1.9\,{\rm K}}\right)^2 \,{\rm cm}^2 \text{ for relativistic } \nu. \end{cases} \tag{9}$$

However, this cross section can produce an acceleration $\sim 10^{-25}$ cm s^{-2} in quite optimistic scenarios [32] which is still less than possible detectable acceleration by order of magnitude.

4.3 Neutrino capture by β-decaying nuclei

Since the current temperature of the relic neutrinos of CνB is $T_{\nu,0} = 1.945\,{\rm K}$, or 1.676×10^{-4} eV, they are extremely non-relativistic and thus do not possess enough threshold energy to be detected in the traditional neutrino detection experiments. An interesting proposal to detect these relic neutrinos is the process of neutrino capture on the β-unstable nuclei [33–35]. The greatest advantage of this process is that the process does not require any threshold energy of the initial state neutrinos. Based on this idea, the PTOLEMY [36] experiment is proposed to use tritium (^{3}H) as the target element since it provides the best chances of CνB detection due to its lifetime, availability, a low Q value and a high neutrino capture cross-section [35]. The process of neutrino capture on ^{3}H is, $\nu_e + {}^3{\rm H} \rightarrow {}^3{\rm He} + e^-$. Recall that in the standard theory of neutrino oscillations, a flavour eigenstate of neutrino ($|\nu_\alpha\rangle$) is expressed as

$$|\nu_\alpha\rangle = \sum_{j=1}^{3} U^*_{\alpha j} |\nu_i\rangle, \tag{10}$$

where, $|\nu_i\rangle$ represent the mass eigenstates, U is the mixing matrix, and in general α can be e, μ or τ corresponding to the three flavors of neutrino. Since here we are only concerned about ν_e the relevant elements of the mixing matrix are U_{ei}. As the relic neutrinos propagate through the universe since the decoupling, they eventually (within $t \sim H_0^{-1}$) decompose into the mass eigenstates [37]. The capture rate of CνB neutrinos by ^{3}H can then be given as, $\Gamma_{\rm C\nu B} = \sum_{j=1}^{3} \Gamma_j$, where Γ_j corresponds to the capture rate of the j-th mass eigenstate of neutrino, which can in turn be expressed as [36],

$$\Gamma_j = N_H |U_{ej}|^2 \int \frac{d^3 p_j}{(2\pi^3)} \sigma(p_j) v_j f_j(p_j) = \; N_H \sigma_j^{\rm SM} v_j f_{c,\,j} n_{\nu,\,0}. \tag{11}$$

Here, $N_H = M_H / m_{\rm H}$ is the number of tritium nuclei in a target mass of M_H, p_j represents the neutrino momentum, v_j is the neutrino velocity as measured at the detector, $\sigma(p_j)$ is the momentum dependent cross-section and $f_j(p_j)$ is the momentum distribution function of the j-th neutrino mass eigenstate. The second equality is due to the approximation of narrow phase space distribution of the CνB neutrinos. The quantity $f_{c,\,j}$ is the neutrino clustering factor due to gravitational attraction of the galactic contents [25, 38, 39]. The average cross-section for neutrino capture according to the SM is,

$$\sigma_j^{\rm SM} v_j = \frac{G_F^2}{2\pi} |V_{ud}|^2 |U_{ej}|^2 F_Z(E_e) \frac{m_{\rm He}}{m_{\rm H}} E_e p_e \left[g_V^2 + 3 g_A^2\right], \tag{12}$$

where, E_e is the electron energy, p_e is the electron momentum, $m_{\rm He} \approx 2808.391\,{\rm MeV}$ and $m_{\rm H} \approx 2808.921\,{\rm MeV}$. The quantities g_V and g_A are the concerned vector and axial-vector couplings. The Fermi function, $F_Z(E_e)$ takes into account the Coulomb interaction between a proton and an outgoing electron. This is can be approximated as

[40],

$$F_Z(E_e) = \frac{2\pi Z\alpha E_e/p_e}{1-\exp(-2\pi Z\alpha E_e/p_e)}. \tag{13}$$

In our concerned case, $Z = 2$ is the atomic number of ^{3}He and $\alpha = 1/137.036$ is the fine structure constant. In the expressions of the capture rate and cross-section, the mixing parameter $|U_{ej}|^2$ appears because even though the neutrinos propagate in their mass eigenstates they are expected to be captured in their flavor eigenstate, i.e. ν_e.

One of the crucial background of CνB neutrino capture is the electrons of the highest energy produced from the β-decay of tritium itself. To take this into account, we express the β decay spectrum as [36, 41],

$$\frac{\mathrm{d}\Gamma_\beta}{\mathrm{d}E_e} = \frac{N_H}{\pi^2}\sum_{j=1}^{3}\sigma_j^{\mathrm{SM}}H(E_e, m_j), \tag{14}$$

where,

$$H(E_e, m_j) = \frac{1-m_e^2/(E_e m_{\mathrm{H}})}{(1-2E_e/m_{\mathrm{H}}+m_e^2/m_{\mathrm{H}}^2)^2}\sqrt{y\left(y+\frac{2m_j m_{\mathrm{He}}}{m_{\mathrm{H}}}\right)}\left[y+\frac{m_j}{m_{\mathrm{H}}}(m_{\mathrm{He}}+m_j)\right], \tag{15}$$

for $y = E_{\mathrm{end},0} - E_e - m_j$, and $E_{\mathrm{end},0}$ is the β-decay endpoint energy for neutrinos with zero mass.

It must be noted that the experimental energy resolution Δ plays a pivotal role in the detection of CνB. The effect of Δ can be incorporated into the calculation by convoluting both the CνB and β-decay part of the electron spectrum with a Gaussian of full width at half maximum given by Δ, which in turn smears the electron spectrum. The smeared β-decay spectrum is expressed as,

$$\frac{\mathrm{d}\bar{\Gamma}_\beta}{\mathrm{d}E_e}(E_e) = \frac{1}{\sqrt{2\pi}(\Delta/\sqrt{8\ln 2})}\int_{-\infty}^{+\infty}\mathrm{d}E'\frac{d\Gamma_\beta}{\mathrm{d}E_e}(E')\exp\left[-\frac{(E_e-E')^2}{2\left(\Delta/\sqrt{8\ln 2}\right)^2}\right]. \tag{16}$$

Similarly, the smeared CνB neutrino capture rate can be expressed as,

$$\frac{d\bar{\Gamma}_{\mathrm{C}\nu\mathrm{B}}}{dE_e}(E_e) = \frac{1}{\sqrt{2\pi}(\Delta/\sqrt{8\ln 2})}\sum_{j=1}^{3}\Gamma_j\exp\left[-\frac{[E_e-(E_{\mathrm{end}}+m_j+m_{\mathrm{lightest}})]^2}{2(\Delta/\sqrt{8\ln 2})^2}\right], \tag{17}$$

where $E_{\mathrm{end}} = E_{\mathrm{end},0} - m_{\mathrm{lightest}}$ is the endpoint energy of the β-decay, m_{lightest} being the mass of the lightest neutrino. Depending on the resolution of the detector, these expressions for the electron spectrum produce the typical gap between the β-decay and neutrino capture spectrum that is connected to the lightest mass of the neutrino eigenstates.

In the remaining part of this article, we are going to discuss the effect of generalized neutrino interactions on the observations of PTOLEMY. This is largely based on [42].

5 Generalized neutrino interaction at PTOLEMY

5.1 Basics of generalized neutrino Interaction

Interactions of neutrinos with matter can lead to neutrino non-standard interactions (NSI)—a type of *new physics* interactions beyond just the mass generation—which may appear in unknown couplings [43]. The effective Lagrangian of such interactions is usually expressed in (chiral) vector form as,

$$\mathcal{L}_{NSI}^{NC/CC} \supset \frac{G_F}{\sqrt{2}}\underset{\alpha\beta}{\overset{ff'}{\int}}\left[\bar{\nu}_\alpha\gamma^\rho(1-\gamma^5)\nu_\beta\right]\left[\bar{f}\gamma_\rho(1\mp\gamma^5)f'\right] + h.c., \tag{18}$$

where $\epsilon_{\alpha\beta}^{ff'}$ represent the NSI parameters, f, $f' = e$, u, d, and α, $\beta = e$, μ, τ. For $f = f'$ the NSIs are neutral-current (NC) like, else it is charged-current (CC) like. However, this can be even more generalised to include the

Table 1 GNI parameters and the Lorentz structures corresponding to them relevant in this study

ϵ_{lq}	$\mathcal{O}_l$	$\mathcal{O}_q$
ϵ_{LL}	$\gamma^\mu(1-\gamma^5)$	$\gamma_\mu(1-\gamma^5)$
ϵ_{LR}	$\gamma^\mu(1-\gamma^5)$	$\gamma_\mu(1+\gamma^5)$
ϵ_{RL}	$\gamma^\mu(1+\gamma^5)$	$\gamma_\mu(1-\gamma^5)$
ϵ_{RR}	$\gamma^\mu(1+\gamma^5)$	$\gamma_\mu(1+\gamma^5)$
ϵ_{LS}	$1-\gamma^5$	1
ϵ_{RS}	$1+\gamma^5$	1
ϵ_{LT}	$\sigma^{\mu\nu}(1-\gamma^5)$	$\sigma_{\mu\nu}(1-\gamma^5)$
ϵ_{RT}	$\sigma^{\mu\nu}(1+\gamma^5)$	$\sigma_{\mu\nu}(1+\gamma^5)$

Lorentz-invariant interactions beyond the usual chiral and vector-like form of the NSIs, these are called *generalized neutrino interactions* (GNI) [44]. Since, we are interested to study the effect of GNIs in relic neutrino capture on β-decaying tritium, expressing the effective Lagrangian in mass eigenstates is more appropriate to obtain the relevant interactions,

$$\mathcal{L}_{eff} = -\frac{G_F}{\sqrt{2}} V_{ud} U_{ej} \left\{ \left[\bar{e}\gamma^\mu(1-\gamma^5)\nu_j\right]\left[\bar{u}\gamma_\mu(1-\gamma^5)d\right] + \sum_{l,\,q} \int_{lq} [\bar{e}\mathcal{O}_l\nu_j][\bar{u}\mathcal{O}_q d] \right\} + h.c., \tag{19}$$

where the dimensionless couplings ϵ_{lq} represent the GNI parameters and $j = 1, 2, 3$ are the three mass eigenstates of neutrino. The operators $\mathcal{O}_l$ and $\mathcal{O}_q$ are the relevant lepton and quark current, respectively, and are given in Table 1. The quantities V_{ud} and U_{ej} are the relevant elements of the Cabibbo–Kobayashi–Maskawa (CKM) and Pontecorvo–Maki–Nakagawa–Sakata (PMNS) matrices, respectively. In this study, we have conducted an analysis considering both left- and right-handed neutrinos in a model-independent manner. This approach allows us to explore scenarios where neutrino mass can be either of Dirac or Majorana nature.

One can express the relevant hadronic matrix elements corresponding to the quark current mentioned in Eq. (19) and Table 1 as [45–47],

$$\langle p(p_p)|\bar{u}d|n(p_n)\rangle = g_S\left(q^2\right)\overline{u_p}(p_p)u_n(p_n), \tag{20a}$$

$$\left\langle p(p_p)\middle|\bar{u}\sigma^{\mu\nu}\left(1\pm\gamma^5\right)d\middle|n(p_n)\right\rangle = g_T\left(q^2\right)\overline{u_p}(p_p)\sigma^{\mu\nu}\left(1\pm\gamma^5\right)u_n(p_n), \tag{20b}$$

$$\left\langle p(p_p)\middle|\bar{u}\gamma^\mu\left(1\pm\gamma^5\right)d\middle|n(p_n)\right\rangle = \overline{u_p}(p_p)\gamma^\mu\left[g_V\left(q^2\right)\pm g_A\left(q^2\right)\gamma^5\right]u_n(p_n). \tag{20c}$$

Though these form-factors depend on the transferred momentum $q^2 = (p_n - p_p)^2$, for the capture rate of the non-relativistic CνB neutrinos one can safely take the limit $q^2 \sim 0$. Here, g_V, g_A, g_S, and g_T correspond to the form-factors of vector, axial-vector, pseudo-scalar and tensor Lorentz structures, respectively. The values of the form-factors used in our analysis is given in Table 2.

The relic neutrino capture cross-section in the presence of GNI for a neutrino mass-eigenstate j, with helicity $h_j = \pm 1$ and velocity v_j can be expressed as [24],

$$\sigma_j^{BSM}(h_j)v_j = \frac{G_F^2}{2\pi}|V_{ud}|^2|U_{ej}|^2\ F_Z(E_e)\frac{m_{He}}{m_H}E_e p_e \mathcal{M}_j(\in_{lq}), \tag{21}$$

Table 2 Values of the hadronic form factors used in this work

Form Factor	Value	References
$g_V(0)$	1	[48, 49]
$\tilde{g}_A(0)/g_V(0)$	1.278 ± 0.0021	[50]
$g_S(0)$	1.02 ± 0.11	[51]
$g_T(0)$	1.020 ± 0.076	[52]

where $\mathcal{M}_j(\epsilon_{lq})$ is the amplitude-squared and it carries the information of the GNI parameters ϵ_{lq}.

We like to point out that all GNI terms tabulated in Table 1 cannot be tested using only (inverse) β-decay experiments. This is due to the fact that the vector and axial-vector GNIs come along with SM couplings and hence can be absorbed in the CKM matrix elements. Thus, probing ϵ_{LL}, ϵ_{LR}, ϵ_{RL}, and ϵ_{RR} is not possible, see [42] for more details. Therefore we stick to only the scalar and tensor BSM interactions on capture cross section to determine their effects on the electron spectrum due to CνB capture.

5.2 Numerical analysis

We now present the methodology to characterize the sensitivity of the PTOLEMY detector to determine statistical bounds on the GNI parameters. We perform a χ^2-analysis by adopting the technique developed in [53]. We start our simulation by evaluating the number of β-decays (N^i_β) and the relic neutrino capture events ($N^i_{\rm CNB}$) as [36],

$$N^i_\beta = \; T\int_{E_i-\delta/2}^{E_i+\delta/2}\frac{d\bar{\Gamma}_\beta}{dE_e}dE_e \; , \; N^i_{CNB} = T\int_{E_i-\delta/2}^{E_i+\delta/2}\frac{d\bar{\Gamma}_{CNB}}{dE_e}dE_e, \tag{22}$$

where E_i is the energy of the i-th bin which has width δ, T is the exposure time and we fix $\delta = 10$ meV. The differential capture rates are given by Eqs. (16) and (17). Here, these event numbers are basically functions of the endpoint energy of β-decay spectrum, $E_{\rm end}$, the parameters of the leptonic mixing matrix, U, and the active neutrino masses, m_i. We estimate the number of expected events for a given bin to be the sum of these events,

$$N^i(E_{end},\, m_j,\, U_{ej}) = N^i_\beta(E_{end},\, m_j,\, U_{ej}) + N^i_{CNB}(E_{end},\, m_j,\, U_{ej}). \tag{23}$$

Eventually, the total number of events in a given energy bin is calculated by taking into account the constant background events, $N_{\rm Bkg}$, which can be read as

$$N^i_{\rm tot}(E_{\rm end},\, m_j,\, U_{ej}) = N^i(E_{\rm end},\, m_j,\, U_{ej}) + N_{\rm Bkg}. \tag{24}$$

In a PTOLEMY-like experiment for the purpose of our study, the number of background events in the region around the endpoint energy is $\mathcal{O}(1)$, as we are assuming a background decay rate of 10^{-5} Hz in the 15 eV energy range around the endpoint energy [36]. Next, we use the Asimov data set [54] i.e., the dataset where there are no statistical fluctuations around the calculated number of events to estimate the experimental measurement in each energy bin,

$$N^i_{\rm exp}(E_{\rm end},\, m_j,\, U_{ej}) = N^i_{\rm tot}(E_{\rm end},\, m_j,\, U_{ej}) \pm \sqrt{N^i_{\rm tot}(E_{\rm end},\, m_j,\, U_{ej})}, \tag{25}$$

where we have assumed a statistical error of $\sqrt{N^i_{\rm tot}}$.

Following a similar process to calculate the number of events for the standard scenario, the expected number of events in the presence of GNIs can be expressed as,

$$N^i_{GNI-th}(E_{end},\, m_j,\, U_{ej},\, \in_{lq}) = N^i_\beta(E_{end},\, m_j,\, U_{ej}) + N^i_{GNI-CNB}(E_{end},\, m_j,\, U_{ej},\, \in_{lq}) + N_{Bkg}, \tag{26}$$

where $N^i_{\text{GNI-CNB}}(E_{\rm end},\, m_j,\, U_{ej},\, \epsilon_{lq})$ is the number of events in each energy bin of width Δ around the energy E_i during an exposure time T for relic neutrino capture in presence of GNI. With this prescription, we define the expression of χ^2 as,

$$\chi^2 = \sum_i \left(\frac{N^i_{\rm exp}(E_{\rm end},\, m_j,\, U_{ej}) - N^i_{\text{GNI-th}}(E_{\rm end},\, m_j,\, U_{ej},\, \epsilon_{lq})}{\sqrt{N^i_{\rm tot}}} \right)^2. \tag{27}$$

Recall that $N^i_{\text{GNI-th}}$ represents the theoretical number of events in the presence of GNIs, whereas $N^i_{\rm exp}$ means the experimental data in the absence of new physics, i.e., just the SM expectation. In our numerical analysis, we have used the neutrino oscillation data from [55, 56]. Here we just show the one-parameter analysis, the two-parameter study can be found in [42].

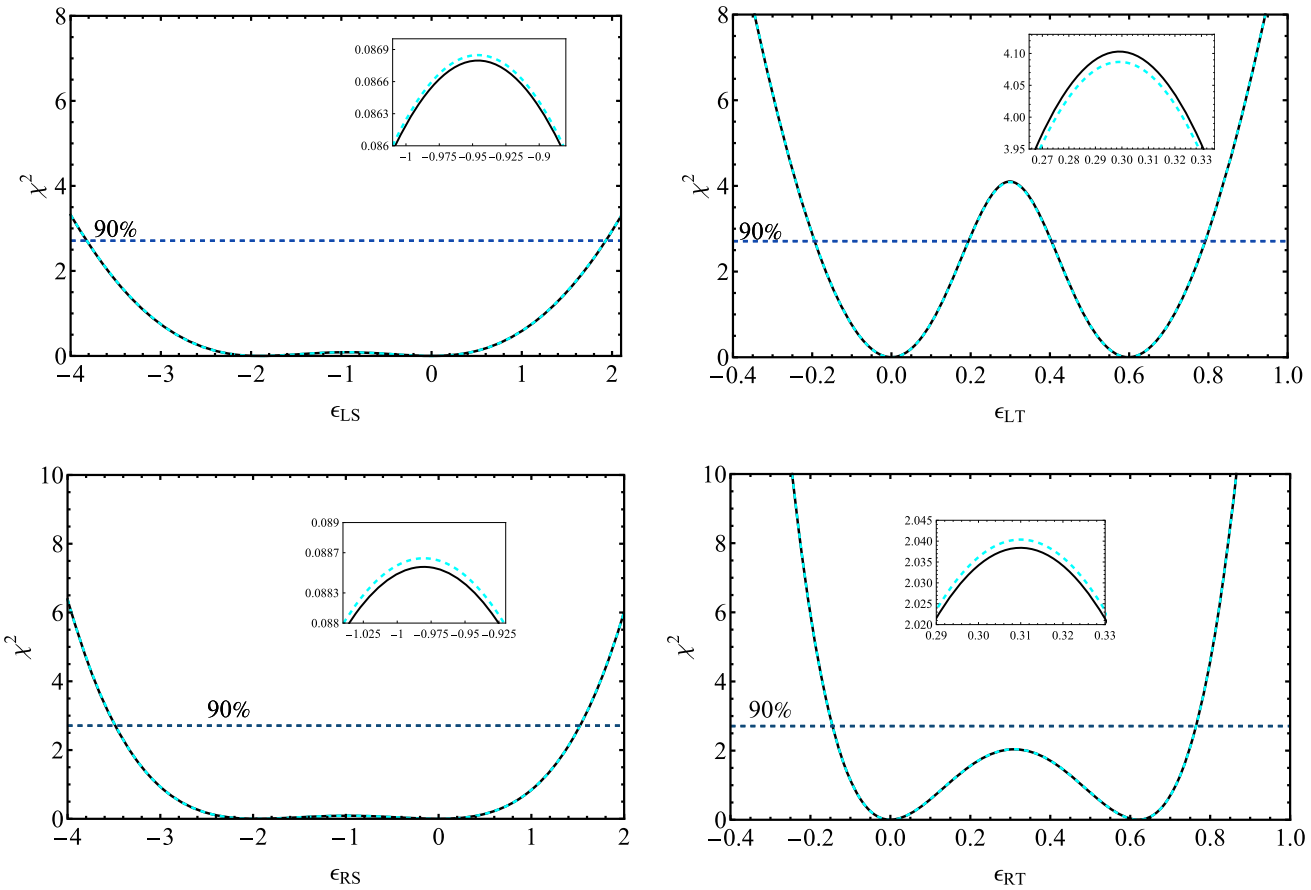

Fig. 1 χ^2 vs ϵ_{lq} for $l = L, R$ and $q = S, T$. Here, the solid black (dashed cyan) line corresponds to the normal (inverted) neutrino mass ordering, whereas the horizontal dotted blue line represents the 90% confidence level. The difference between the χ^2 values for the different mass orderings has been shown in the insets

5.2.1 One-parameter analysis

We perform the χ^2 analysis considering one non-zero GNI parameter at a time following Eq. (27). The results are presented for the normal and inverted neutrino mass ordering in Fig. 1 using the solid black and dotted cyan lines, respectively.

By observing all the panels, it can be noted that a value of $\epsilon_{lq} = 0$ fits the data (i.e., for no new physics contribution) in the same way, a value of $\epsilon_{lq} \neq 0$ resembles the measured signal due to a partial destructive interference with the SM value. From the analytic form of the amplitude-squared, this feature can be understood analytically. The bottom right plot of Fig. 1 shows the presence of intrinsic degeneracy for ϵ_{RT}. The PTOLEMY experiment with its future data can not remove such intrinsic degeneracy. Likewise, the presence of degeneracy for other GNI parameters can also be understood from the remaining panels. The values where the degeneracies occur in χ^2 values for ϵ_{LT} is (0, 0.6). We notice further that the degeneracy is discrete for the top-right panel at 90% confidence level (CL) i.e., the complete allowed parameter regions are not below the horizontal blue dashed line for ϵ_{LT}. On the other hand, the allowed regions are below the horizontal blue dashed line for the other three panels, and that leads to a continuous degeneracy to ϵ_{RT}, ϵ_{RS} and ϵ_{LS}, respectively.

We also observe that the PTOLEMY can put the most stringent constraints on ϵ_{LT} as can be seen from the top-right panel at 90% CL. The bounds at 90% CL are summarized in Table 3.

5.3 Electron spectrum in the presence GNI

One crucial physical observable in the neutrino capture method is the electron spectrum from $\nu_e + {}^3\mathrm{H} \rightarrow {}^3\mathrm{He} + e^-$. It is to be noted that for massive neutrinos, the endpoint energy of the β-decay background is less than the endpoint energy of a massless case and they are related as,

$$E_{\mathrm{end,\,massive}} = E_{\mathrm{end},\,0} - m_{\mathrm{lightest}}. \tag{28}$$

Table 3 Allowed values of different GNI parameters, ϵ_{QX} ($Q = L,\ R,\ X = S,\ T$), corresponding to the 90% CL obtained from Fig. 1

GNI Parameter	χ^2 values at 90% CL
ϵ_{LS}	$[-3.8,\ 1.9]$
ϵ_{LT}	$[-0.19,\ 0.19]$, $[0.4,\ 0.8]$
ϵ_{RS}	$[-3.5,\ 1.5]$
ϵ_{RT}	$[-0.15,\ 0.75]$

In Fig. 2, we have shown the electron spectrum of neutrino capture on tritium around the endpoint energy of β-decay for the SM as well as in the presence of GNIs (see figure caption for color details).

We show the scenario in the absence of finite experimental resolution i.e., for $\Delta = 0$ using the dotted blue and red lines for both the mass orderings. We observe a sharp drop in the β-decay spectrum from all four panels. For a realistic experimental set-up, we have smeared the signal with respect to a finite experimental resolution of $\Delta = 20\,\text{meV}$, due to which the β-decay background goes beyond the endpoint energy. For the electron spectrum due to the capture of ν_e, the spectrum peaks beyond the endpoint energy of the β-decay of tritium.

To show the impact of GNI parameters on the electron spectrum of CNB capture in a comprehensive manner, we describe our results in four panels of Fig. 2 considering one non-zero GNI parameter at a time. The benchmark values of GNI parameters that are used here are taken from Table 3. The computed electron spectrum corresponds to fixed values of $m_{\text{lightest}} = 50\,\text{meV}$ and $\Delta = 20\,\text{meV}$. We notice from all four panels that the peak of the electron spectrum is at $m_{\text{lightest}} = 50\,\text{meV}$ for normal neutrino mass ordering (NO), whereas it is at a slightly higher value for inverted ordering (IO). This can be understood from Eq. (17). Note that the capture rate peaks at $E_e - E_{\text{end},0} = m_j$. For NO, $j = 1$ and hence one gets maximum contribution for Γ_1 as it depends on U_{e1} using oscillation data. For IO, $j = 3$ we find the least contribution from Γ_3 using oscillation data on U_{e3}.

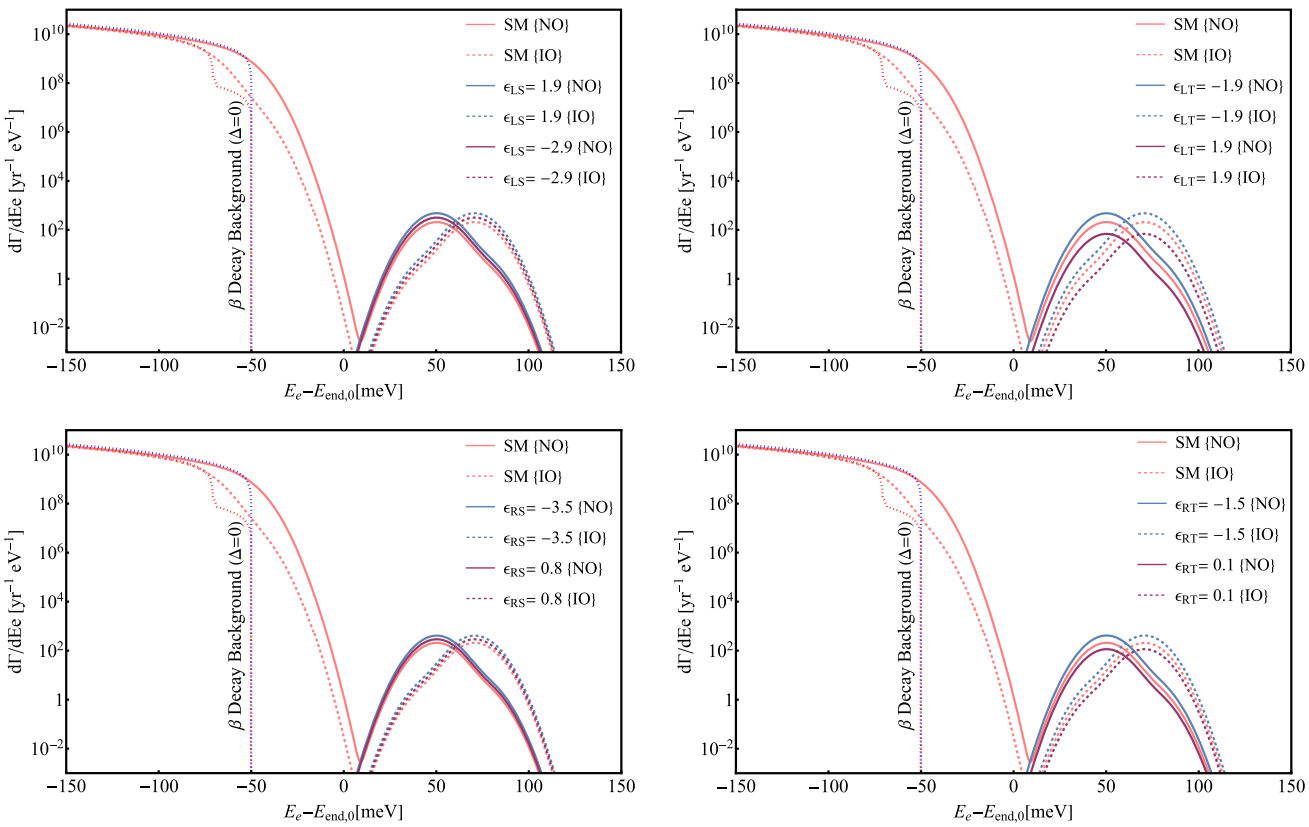

Fig. 2 The electron spectrum near the end point energy of β-decay in the presence and absence of GNI for both the mass orderings. The four different plots have four different GNI parameters i.e. ϵ_{LS}, ϵ_{LT}, ϵ_{RS} and ϵ_{RT}. Here for all four plots $m_{\text{lightest}} = 50\,\text{meV}$ and $\Delta = 20\,\text{meV}$. The solid (dashed) lines correspond to the normal (inverted) ordering, whereas the dotted blue (red) line signifies the β decay background for the normal (inverted) ordering for $\Delta = 0$

Besides this, in the second panel of the top row, we have shown the effect of ϵ_{LT} on the electron spectrum of CNB capture for two benchmark values $\epsilon_{LT} = -1.9$, and 1.9. For $\epsilon_{LT} = -1.9$, it can be observed that the number of events is ~ 2.3 times higher than the SM scenario, whereas for $\epsilon_{LT} = 1.9$ the number of events is ~ 3.3 times lower than the SM scenario for both NO and IO. Setting all the GNI parameters to zero, except ϵ_{LT}, we notice that the larger impact arises for $\epsilon_{LT} = -1.9$ than the SM, whereas the impact is minimum for $\epsilon_{LT} = 1.9$. Similar conclusions can also be made by observing other panels. This shows us that the response function of a PTOLEMY-like experiment is equipped to probe the presence or absence of GNIs' effects. It is also interesting that for the values of the GNI parameters which were used in this study, for most cases, the difference between the two scenarios is significant. We must mention one crucial caveat here that the experimental resolution Δ must be greater than the lightest neutrino mass m_{lightest} to have a distinct signature of the CNB capture from the usual β-decay background. For a correlation between the m_{lightest} and the four different GNI parameters see [42].

6 Summary and future prospects

The existence of CνB is one of the robust preictions of the standard cosmological theory of ΛCDM. Detecting it, on the other, hand is extremely challanging due to the ultra-low energy and weak interaction of the CνB neutrinos. There are quite a few experimental and astrophysical/cosmological observations that can indirectly impose some restrictions on the CνB. As for direct detection, over the decades many interesting proposals are made. We discuss some of these proposals, their pros and cons. We finally discuss, in detail, the most promising of all the proposals i.e., the method of neutrino capture by the β-decaying nuclei. Due to its novel features it is already planned to be employed in PTOLEMY experiment. We discuss some details of the working principles of this experiment and how the signal can be distinguished from the usual β-decay background under which conditions. In the last part of this article, we focused on the very general interactions of neutrinos, namely GNIs. We showed how the presence of GNIs, which can be mimicked by many well-motivated beyond the Standard Model (BSM) scenarios, can affect the observations at the PTOLEMY. Finally, a detection of CνB neutrinos will not only can shed new light on BSM physics but more importantly it can help us hark back to the initial ages of the Universe which is still unseen by humankind.

Acknowledgements UKD thanks I K Banerjee for useful discussions. A clarifying comment from the anonymous referee is also acknowledged.

Data availability This manuscript has no associated data or the data will not be deposited. [Authors' comment: This is a theoretical study and no experimental data has been used.]

References

1. R.H. Dicke, P.J.E. Peebles, P.G. Roll, D.T. Wilkinson, Cosmic black-body radiation. Astrophys. J. **142**, 414–419 (1965). https://doi.org/10.1086/148306
2. S. Weinberg, Universal neutrino degeneracy. Phys. Rev. **128**, 1457–1473 (1962). https://doi.org/10.1103/PhysRev.128.1457
3. E. Baracchini et al., PTOLEMY: a proposal for thermal relic detection of massive neutrinos and directional detection of MeV dark matter (2018) arXiv:1808.01892 [physics.ins-det]
4. L. Stodolsky, Speculations on detection of the neutrino sea. Phys. Rev. Lett. **34**, 110 (1975). https://doi.org/10.1103/PhysRevLett.34.110. (**Erratum: Phys. Rev. Lett. 34, 508 (1975)**)
5. G. Duda, G. Gelmini, S. Nussinov, Expected signals in relic neutrino detectors. Phys. Rev. D **64**, 122001 (2001). https://doi.org/10.1103/PhysRevD.64.122001. arXiv:hep-ph/0107027
6. V. Domcke, M. Spinrath, Detection prospects for the Cosmic Neutrino Background using laser interferometers. JCAP **06**, 055 (2017). https://doi.org/10.1088/1475-7516/2017/06/055. arXiv:1703.08629 [astro-ph.CO]
7. C.S. Nugroho, probing cosmic neutrino background charge via unconventional interferometer (2023) arXiv:2302.08246 [hep-ph]
8. K. Asteriadis, A.Q. Triviño, M. Spinrath, Bremsstrahlung from the cosmic neutrino background (2022) arXiv:2208.01207 [hep-ph]
9. B.R. Safdi, M. Lisanti, J. Spitz, J.A. Formaggio, Annual modulation of cosmic relic neutrinos. Phys. Rev. D **90**(4), 043001 (2014). https://doi.org/10.1103/PhysRevD.90.043001. arXiv:1404.0680 [astro-ph.CO]
10. R. Opher, Coherent scattering of cosmic neutrinos. Astron. Astrophys. **37**(1), 135–137 (1974)
11. R.R. Lewis, Coherent detector for low-energy neutrinos. Phys. Rev. D **21**, 663 (1980). https://doi.org/10.1103/PhysRevD.21.663

12. V.F. Shvartsman, V.B. Braginskii, S.S. Gershtein, I.B. Zeldovich, M.I. Khlopov, Possibility of detecting relict massive neutrinos. ZhETF Pisma Redaktsiiu **36**, 224–226 (1982)
13. J.D. Shergold, Updated detection prospects for relic neutrinos using coherent scattering. JCAP **11**(11), 052 (2021). https://doi.org/10.1088/1475-7516/2021/11/052. arXiv:2109.07482 [hep-ph]
14. V. Brdar, P.S.B. Dev, R. Plestid, A. Soni, A new probe of relic neutrino clustering using cosmogenic neutrinos. Phys. Lett. B **833**, 137358 (2022). https://doi.org/10.1016/j.physletb.2022.137358. arXiv:2207.02860 [hep-ph]
15. M. Yoshimura, N. Sasao, M. Tanaka, Experimental method of detecting relic neutrino by atomic de-excitation. Phys. Rev. D **91**(6), 063516 (2015). https://doi.org/10.1103/PhysRevD.91.063516. arXiv:1409.3648 [hep-ph]
16. M. Bauer, J.D. Shergold, Relic neutrinos at accelerator experiments. Phys. Rev. D **104**(8), 083039 (2021). https://doi.org/10.1103/PhysRevD.104.083039. arXiv:2104.12784 [hep-ph]
17. J.L. Bernal, A. Caputo, F. Villaescusa-Navarro, M. Kamionkowski, Searching for the radiative decay of the cosmic neutrino background with line-intensity mapping. Phys. Rev. Lett. **127**(13), 131102 (2021). https://doi.org/10.1103/PhysRevLett.127.131102. arXiv:2103.12099 [hep-ph]
18. D.A. Dicus, E.W. Kolb, A.M. Gleeson, E.C.G. Sudarshan, V.L. Teplitz, M.S. Turner, Primordial nucleosynthesis including radiative, coulomb, and finite temperature corrections to weak rates. Phys. Rev. D **26**, 2694 (1982). https://doi.org/10.1103/PhysRevD.26.2694
19. K. Enqvist, K. Kainulainen, V. Semikoz, Neutrino annihilation in hot plasma. Nucl. Phys. B **374**, 392–404 (1992). https://doi.org/10.1016/0550-3213(92)90359-J
20. S. Dodelson, M.S. Turner, Nonequilibrium neutrino statistical mechanics in the expanding universe. Phys. Rev. D **46**, 3372–3387 (1992). https://doi.org/10.1103/PhysRevD.46.3372
21. S. Hannestad, J. Madsen, Nucleosynthesis and the mass of tau-neutrino revisited. Phys. Rev. D **54**, 7894–7897 (1996). https://doi.org/10.1103/PhysRevD.54.7894
22. K. Akita, M. Yamaguchi, A precision calculation of relic neutrino decoupling. JCAP **08**, 012 (2020). https://doi.org/10.1088/1475-7516/2020/08/012. arXiv:2005.07047 [hep-ph]
23. D.J. Fixsen, The temperature of the cosmic microwave background. Astrophys. J. **707**, 916–920 (2009). https://doi.org/10.1088/0004-637X/707/2/916. arXiv:0911.1955 [astro-ph.CO]
24. A.J. Long, C. Lunardini, E. Sabancilar, Detecting non-relativistic cosmic neutrinos by capture on tritium: phenomenology and physics potential. JCAP **08**, 038 (2014). https://doi.org/10.1088/1475-7516/2014/08/038. arXiv:1405.7654 [hep-ph]
25. A. Ringwald, Y.Y.Y. Wong, Gravitational clustering of relic neutrinos and implications for their detection. JCAP **12**, 005 (2004). https://doi.org/10.1088/1475-7516/2004/12/005. arXiv:hep-ph/0408241
26. P. Mertsch, G. Parimbelli, P.F. Salas, S. Gariazzo, J. Lesgourgues, S. Pastor, Neutrino clustering in the Milky Way and beyond. JCAP **01**, 015 (2020). https://doi.org/10.1088/1475-7516/2020/01/015. arXiv:1910.13388 [astro-ph.CO]
27. M. Bauer, J.D. Shergold, Limits on the cosmic neutrino background. JCAP **01**, 003 (2023). https://doi.org/10.1088/1475-7516/2023/01/003. arXiv:2207.12413 [hep-ph]
28. S. Kumaran et al., First direct evidence of the CNO fusion cycle in the Sun with Borexino. PoS ICRC2021, 1109 (2021) https://doi.org/10.22323/1.395.1109
29. D. Baumann, F. Beutler, R. Flauger, D. Green, A. Slosar, M. Vargas-Magaña, B. Wallisch, C. Yèche, First constraint on the neutrino-induced phase shift in the spectrum of baryon acoustic oscillations. Nat. Phys. **15**, 465–469 (2019). https://doi.org/10.1038/s41567-019-0435-6. arXiv:1803.10741 [astro-ph.CO]
30. R. Mohammadi, J. Khodagholizadeh, M. Sadegh, S.-S. Xue, B-mode polarization of the CMB and the cosmic neutrino background. Phys. Rev. D **93**(12), 125029 (2016). https://doi.org/10.1103/PhysRevD.93.125029. arXiv:1602.00237 [astro-ph.CO]
31. E. Vitagliano, I. Tamborra, G. Raffelt, Grand unified neutrino spectrum at earth: sources and spectral components. Rev. Mod. Phys. **92**, 45006 (2020). https://doi.org/10.1103/RevModPhys.92.045006. arXiv:1910.11878 [astro-ph.HE]
32. C. Yanagisawa, Looking for cosmic neutrino background. Front. Phys. **2**, 30 (2014). https://doi.org/10.3389/fphy.2014.00030
33. S. Weinberg, *Gravitation and cosmology: principles and applications of the general theory of relativity* (Wiley, New York, 1972)
34. A.G. Cocco, G. Mangano, M. Messina, Low energy antineutrino detection using neutrino capture on EC decaying nuclei. Phys. Rev. D **79**, 053009 (2009). https://doi.org/10.1103/PhysRevD.79.053009. arXiv:0903.1217 [hep-ph]
35. A.G. Cocco, G. Mangano, M. Messina, Probing low energy neutrino backgrounds with neutrino capture on beta decaying nuclei. JCAP **06**, 015 (2007). https://doi.org/10.1088/1475-7516/2007/06/015. arXiv:hep-ph/0703075
36. M.G. Betti et al., Neutrino physics with the PTOLEMY project: active neutrino properties and the light sterile case. JCAP **07**, 047 (2019). https://doi.org/10.1088/1475-7516/2019/07/047. arXiv:1902.05508 [astro-ph.CO]
37. T.J. Weiler, Relic neutrinos, Z bursts, and cosmic rays above 10**20-eV. In: 2nd International Conference Physics Beyond the Standard Model: Beyond the Desert 99: Accelerator, Nonaccelerator and Space Approaches, pp. 1085–1106 (1999)
38. P.F. Salas, S. Gariazzo, J. Lesgourgues, S. Pastor, Calculation of the local density of relic neutrinos. JCAP **09**, 034 (2017). https://doi.org/10.1088/1475-7516/2017/09/034. arXiv:1706.09850 [astro-ph.CO]
39. J. Zhang, X. Zhang, Gravitational clustering of cosmic relic neutrinos in the Milky Way. Nat. Commun. **9**, 1833 (2018). https://doi.org/10.1038/s41467-018-04264-y. arXiv:1712.01153 [astro-ph.CO]

40. H. Primakoff, S.P. Rosen, Double beta decay. Rept. Prog. Phys. **22**(1), 121–166 (1959). https://doi.org/10.1088/0034-4885/22/1/305
41. S.S. Masood, S. Nasri, J. Schechter, M.A. Tortola, J.W.F. Valle, C. Weinheimer, Exact relativistic beta decay endpoint spectrum. Phys. Rev. C **76**, 045501 (2007). https://doi.org/10.1103/PhysRevC.76.045501. arXiv:0706.0897 [hep-ph]
42. I.K. Banerjee, U.K. Dey, N. Nath, S.S. Shariff, Testing generalized neutrino interactions with PTOLEMY (2023) arXiv:2304.02505 [hep-ph]
43. L. Wolfenstein, Neutrino oscillations in matter. Phys. Rev. D **17**, 2369–2374 (1978). https://doi.org/10.1103/PhysRevD.17.2369
44. M. Lindner, W. Rodejohann, X.-J. Xu, Coherent Neutrino-Nucleus Scattering and new Neutrino Interactions. JHEP **03**, 097 (2017). https://doi.org/10.1007/JHEP03(2017)097. arXiv:1612.04150 [hep-ph]
45. S. Weinberg, Charge symmetry of weak interactions. Phys. Rev. **112**, 1375–1379 (1958). https://doi.org/10.1103/PhysRev.112.1375
46. V. Cirigliano, S. Gardner, B. Holstein, Beta decays and non-standard interactions in the LHC era. Prog. Part. Nucl. Phys. **71**, 93–118 (2013). https://doi.org/10.1016/j.ppnp.2013.03.005. arXiv:1303.6953 [hep-ph]
47. P.O. Ludl, W. Rodejohann, Direct neutrino mass experiments and exotic charged current interactions. JHEP **06**, 040 (2016). https://doi.org/10.1007/JHEP06(2016)040. arXiv:1603.08690 [hep-ph]
48. S.S. Gershtein, Y.B. Zeldovich, Meson corrections in the theory of beta decay. Zh. Eksp. Teor. Fiz. **29**, 698–699 (1955)
49. R.P. Feynman, M. Gell-Mann, Theory of Fermi interaction. Phys. Rev. **109**, 193–198 (1958). https://doi.org/10.1103/PhysRev.109.193
50. E. Berkowitz et al., An accurate calculation of the nucleon axial charge with lattice QCD (2017) arXiv:1704.01114 [hep-lat]
51. M. González-Alonso, J. Martin Camalich, Isospin breaking in the nucleon mass and the sensitivity of β decays to new physics. Phys. Rev. Lett. **112**(4), 042501 (2014). https://doi.org/10.1103/PhysRevLett.112.042501. arXiv:1309.4434 [hep-ph]
52. T. Bhattacharya, V. Cirigliano, R. Gupta, H.-W. Lin, B. Yoon, Neutron electric dipole moment and tensor charges from lattice QCD. Phys. Rev. Lett. **115**(21), 212002 (2015). https://doi.org/10.1103/PhysRevLett.115.212002. arXiv:1506.04196 [hep-lat]
53. J. Angrik et al., KATRIN Design Report (2004)
54. G. Cowan, K. Cranmer, E. Gross, O. Vitells, Asymptotic formulae for likelihood-based tests of new physics. Eur. Phys. J. C **71**, 1554 (2011) https://doi.org/10.1140/epjc/s10052-011-1554-0arXiv:1007.1727 [physics.data-an]. [**Erratum: Eur.Phys.J.C 73, 2501 (2013)**]
55. I. Esteban, M.C. Gonzalez-Garcia, M. Maltoni, T. Schwetz, A. Zhou, The fate of hints: updated global analysis of three-flavor neutrino oscillations. JHEP **09**, 178 (2020). https://doi.org/10.1007/JHEP09(2020)178. arXiv:2007.14792 [hep-ph]
56. NuFit 5.1. http://www.nu-fit.org/. Accessed 9 Dec 2022